Microfluid Nanofluid (2010) 8:549–555
DOI 10.1007/s10404-009-0533-3

SHORT COMMUNICATION

Valveless micropump with acoustically featured pumping chamber

S. S. Wang · X. Y. Huang · C. Yang

Received: 10 September 2009 / Accepted: 11 November 2009 / Published online: 21 November 2009

Abstract This article presents a new design of a valveless micropump. The pump consists of a nozzle-shaped actuation chamber with acoustic resonator profile, which functions as both pumping chamber and flow rectification structure. The pump is fabricated by lamination of layers made of polymethyl-methacrylate (PMMA) and dry adhesives, and is driven by a piezoelectric disk. The performance of the pump has been studied by both experimental characterization and numerical simulations. Both the experimental and numerical results show that the pump works well at low frequencies of 20–100 Hz to produce relatively high backpressures and flowrates. Moreover, the numerical simulations show that in the pumping frequency range, the flow patterns inside the chamber are found to be asymmetric in one pumping cycle so as to create a net flowrate, while outside the pumping frequency range, the flow patterns become symmetric in the pumping cycle. The pumping frequency can be shifted by modifying the pump configuration and dimensions. The pump is suitable for microfluidic integrations.

Keywords Micropump · Microfluidics · Acoustic actuation

1 Introduction

In the last decade, the fast development in life sciences leads to growing importance of microfluidics. Different functions of microfluidic operations, such as pumping and mixing, have to be integrated into a single lab-on-a-chip (LOC). Continuous flow is a good option for pumping reagents in a LOC. Continuous flow in microfluidic channels requires effective pumping of liquids in the microscale. Various kinds of micropumping techniques have therefore been developed. Detailed reviews on micropumps were presented by Nguyen et al. (2002) and Laser and Santiago (2004), covering fabrications, pumping mechanisms, actuations, valves, and operation characteristics, etc. Non-mechanical pumping mechanisms such as electrokinetic pumping for conductive fluids and electrohydrodynamic pumping for dielectric fluids are simple in design, but both concepts depend on the specific properties of pumping fluids. Mechanical pumps require an actuator, which converts the electric energy into mechanical work. Van Lintel et al. (1988) fabricated the first silicon-based micropump that has check-valves in form of a ring diaphragms. Micropumps, such as the peristaltic pumps (Smits 1990), nozzle/diffuser rectification pumps (Stemme and Stemme 1993; Heschel et al. 1997; Jiang et al. 1998; Olsson et al. 2000; Pan et al. 2001), the Tesla-type pumps (Schwesinger et al. 1996; Gray et al. 1999), and acoustic impedance pumps (Lee et al. 2008; Huang et al. 2009), do not need passive check valves. A peristaltic pump consists of three chambers linked in series. By generating peristaltic motion in these chambers, fluids can be pumped in a desired direction. In the nozzle/diffuser micropumps, the flow is rectified due to different pressure drops across the nozzle and the diffuser in different flow directions. Similar to the nozzle/diffuser structures, the Tesla-type pumps apply valvular conduit structures in microscale to generate flow rectification effects without the need of check valves. In the acoustic impedance pumps, the design is to produce an acoustic impedance mismatch between a flexible section and other rigid parts in a microchannel system. By

S. S. Wang · X. Y. Huang (✉) · C. Yang
School of Mechanical and Aerospace Engineering,
Nanyang Technological University, Singapore, Singapore
e-mail: MXHUANG@ntu.edu.sg

actuating the flexible section at certain locations, a standing wave field will be established in the fluid to generate pumping effect. The major problem of these pump concepts is that they require complicated design and complex fabrication processes. Thus, a simple but effective valveless concept is attractive for LOC applications.

In this article, we demonstrate a new design of a planar valveless micropump. In contrast to other valveless pump designs that have separate pump chambers and flow rectification structures, a rather simple nozzle-shape pump chamber has been used in this pump, and the pump chamber in the present design is also used as the flow rectification structure. The pump works stably at driving frequencies less than 100 Hz. Due to its simple design and easy fabrication, the pump can be implemented into many devices with microchannel structures. The actuation is achieved by a piezoelectric disk. Thus the simplicity, reliability and stability of the mechanical hardware are preserved. Besides, since the same design used in the present pump can produce bubbles inside the channel in a higher frequency range 1–2 kHz for flow mixing enhancement (Wang et al. 2009), it is possible to develop a multifunction microfluidic device for both mixing and pumping by simply switching the actuation frequency. The pump performance is characterized in terms of backpressure and flow rates at different driving frequencies. Numerical simulations are also carried out to visualize flow patterns inside the pump chamber and to compute the pumping flow rates. Reasonable agreement is found between the experimental data and the numerical simulations.

2 Pump design, fabrication, and experimental setup

The schematic diagram of the pump is shown in Fig. 1. The major configuration of the pump is adopted from a microfluidic mixer (Wang et al. 2009) which is actuated at high frequencies (>1 kHz) to enhance continuous flow-based micromixing. The pump chamber consists of two parts, a circular chamber to accommodate the piezo disc and an exponentially curved nozzle as shown in Fig. 1a. A similar shape of the chamber has been used for an acoustic resonator (Luo et al. 2007) to achieve high amplitude acoustic pressures. The pump was constructed by two PMMA layers with thicknesses of 1 and 5 mm, and was fabricated using the lamination technology (Wang et al. 2009). A spacer made of a 300-μm thick dry adhesive layer (Adhesives Research, Inc., Arclad 8102 transfer adhesive) formed the pump chamber. The actuation disk was formed by a 15 mm-diameter piezoelectric disk glued to a 22 mm-diameter brass sheet, and was assembled over the circular part of the pump chamber. The diameter of the pump chamber was 16 mm. The brass sheet was directly contacted to the liquid in the

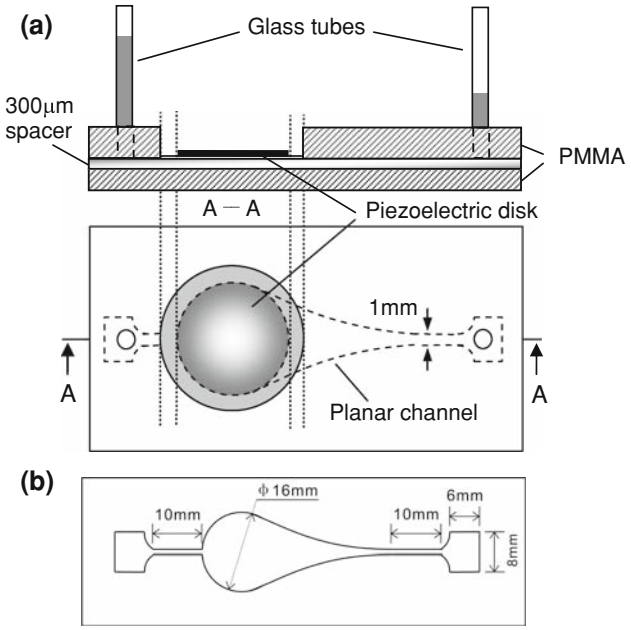

Fig. 1 Schematic diagram of the planar micropump. **a** Basic design and structure, and **b** the pump geometry with dimensions. By setting the axis origin at centre of the circular chamber, the upper-half profile of the pump chamber (y mm) varying with axial position (x mm) is given by algebraic functions $y = \sqrt{8^2 - x^2}$ when $-8 < x \leq 4$ and $y = 0.5e^{0.1011(30-x)}$ when $4 < x \leq 30$

chamber, while the nozzle-shape part was sandwiched between the two PMMA layers. Two 10-mm long and 1-mm wide straight channels connect the pump chamber to the inlet and outlet. Two glass capillaries with inner diameter of 3.5 mm were connected to the inlet and outlet of the pumps through buffer areas. The buffers provide not only proper connections between the planar pump and the vertical capillaries, but also simple flow boundary conditions at the inlet and outlet for the numerical simulations. The glass capillaries and the edge of the piezoelectric disc were sealed by an epoxy to prevent leakage.

Photos of a fabricated pump are shown in Fig. 2a with both the side view and the bottom view, and the experimental setup for the pump characterization is shown in Fig. 2b. The pump was driven by an external signal generator (33120A, Hewlett Packard, USA) and a power amplifier (790, PCB Piezotronics, USA), where the sinusoidal signal from the signal generator was amplified 30 times by the power amplifier.

3 Numerical simulations

Numerical simulations were performed for the pump operations. The simulations followed a two-dimensional model developed by Wu and Lu (2006) for the planar micropumps, in which the fluid was assumed to be a thin

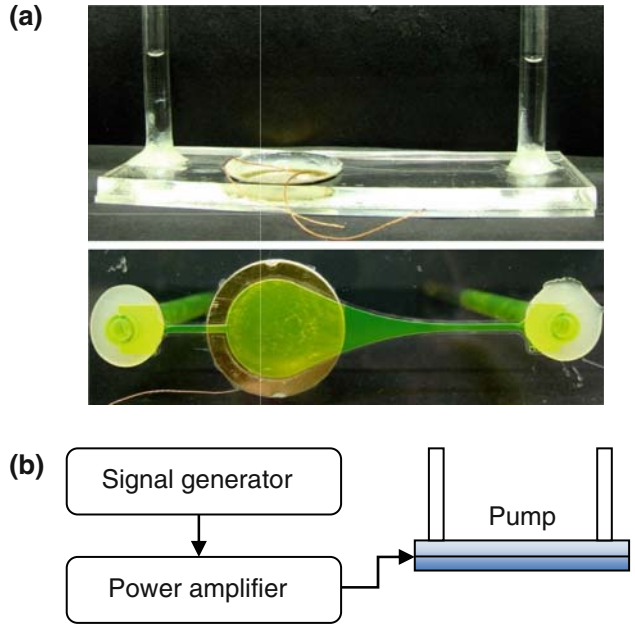

Fig. 2 **a** Photo of a fabricated pump (side and bottom views), and **b** experimental setup for the testing

layer with uniform velocity across the channel height. In the two-dimensional model, the disk actuations are converted into the source terms in both the continuity equation and the Navier–Stokes equation, which are written as

$$\nabla \cdot \mathbf{v} = -\frac{\partial \zeta}{h \partial t}. \tag{1}$$

$$\frac{\partial \mathbf{v}}{\partial t} + \nabla \cdot (\mathbf{vv}) = -\frac{\mathbf{1}}{\rho}\nabla p + \nu \nabla^2 \mathbf{v} + \left\{ \alpha \mathbf{v} - (\mathbf{1} - \beta)\nabla \cdot (\mathbf{vv}) - \frac{\partial \zeta}{\partial t}\frac{\mathbf{v}}{h} \right\}, \tag{2}$$

In Eqs. 1 and 2, $\mathbf{v}$ is the flow velocity in x–y plane, p is the pressure, α is a parameter associated with the fluid viscosity and the channel geometry, β is a parameter associated with the convection terms. The definitions for α and β can be found elsewhere (Wu and Lu 2006) and their values are -25 and 1.2, respectively, in the present simulations. h is the channel height. $\zeta(x, y, t)$ in Eqs. 1 and 2 is a function representing the actuation displacement of the disk on the upper surface of the circular chamber. In the simulation, the actuation displacement is given as (Timoshenko and Woinosky-Krieger 1959)

$$\zeta(x, y, t) = \begin{cases} A_0 \sin(2\pi f)\left(1 - \left(\sqrt{x^2 + y^2}\Big/R\right)^2\right)^2, & \text{within actuation disk;} \\ 0, & \text{outside actuation disk.} \end{cases} \tag{3}$$

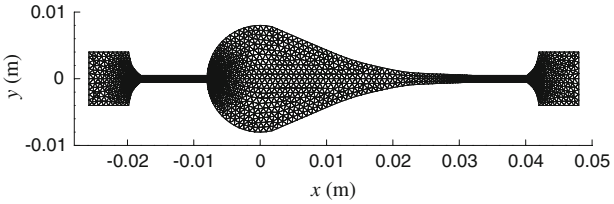

Fig. 3 Meshes used for the numerical simulations

The actuation amplitude, A_0, was measured experimentally from the pump at various actuation frequencies f. Non-uniform meshes were generated over the pumping chamber, the buffers and channels for the simulation, which are illustrated in Fig. 3. In order to capture the detailed flow fields, the meshes were refined in the junctions between the chamber and the channels and the junctions between the buffers and the channel ends. A mesh independent analysis was conducted to ensure reasonably accurate results. The simulations were carried out by using FLUENT with user-defined-function (UDF) for the body force term and the source term. The pressures at the pump inlet and outlet were set to be equal, and the pumping flow rates were calculated by averaging the periodic flow rates over one period.

4 Results and discussion

4.1 Pump performance and experimental characterization

DI water was used as the working fluid. The pumps were characterized by measuring pumping flowrates and backpressures at various driving frequencies and voltages. It was observed that the pumping direction is from the right to left, opposite to the nozzle direction. To measure the maximum backpressure (corresponding to zero flowrate), the glass capillaries were positioned vertically and the backpressure was obtained when no change of the water levels in the glass capillaries was observed. To measure the flowrate at zero backpressure, the glass capillaries were positioned horizontally. By measuring the change of meniscus position of water over a time interval and the capillary diameter, the average flow velocity and flowrates were determined. The frequency characteristics of the

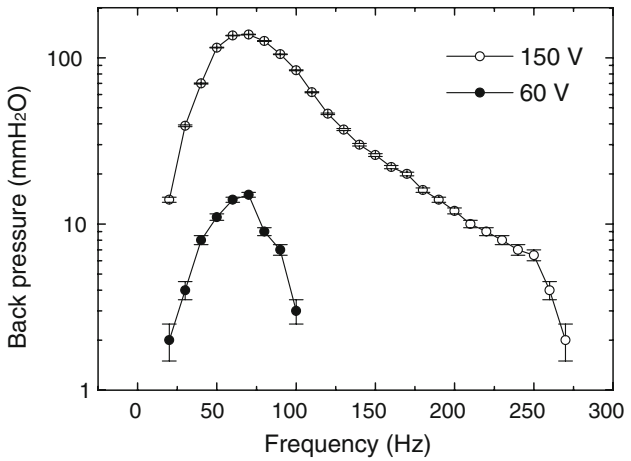

Fig. 4 Measured pumping back pressure versus frequency at 60 and 150 V actuation voltages

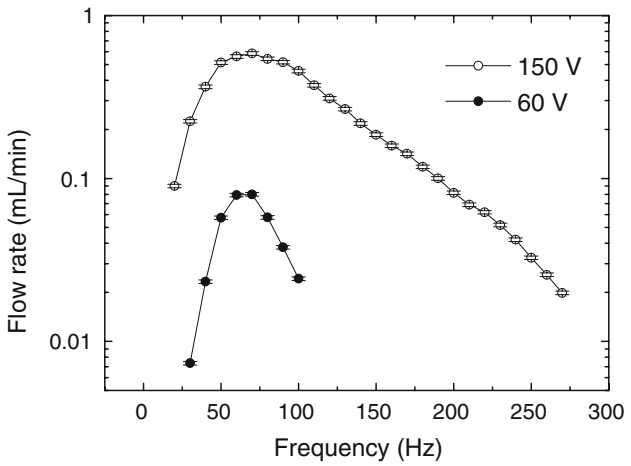

Fig. 5 Measured pumping flow rate versus frequency at 60 and 150 V actuation voltages

pumping backpressure and flowrates are shown in Figs. 4 and 5 for the actuation voltages 60 and 150 V, respectively. It is seen that the pump produces maximum flowrate and backpressures around 70 Hz, and there are almost no pumping effect when the actuation frequencies are greater than 250 Hz or below 20 Hz. The maximum pumping backpressure and flowrate are around 140 mm H_2O and 0.6 ml/min under 150 V actuation voltage.

In order to further investigate the frequency characteristics of the pump, the dynamics of the piezoelectric disk was examined. The disk deflections and velocities were measured using a surface amplitude probe (ADE Technologies Microsense Probe 5130). The probe was pointed to the disk centre so that the results were corresponding to the disk deflections at the centre. The resonance frequency of the actuation disk was examined in the frequency range 0–10 kHz. The measured results showed that, for the empty

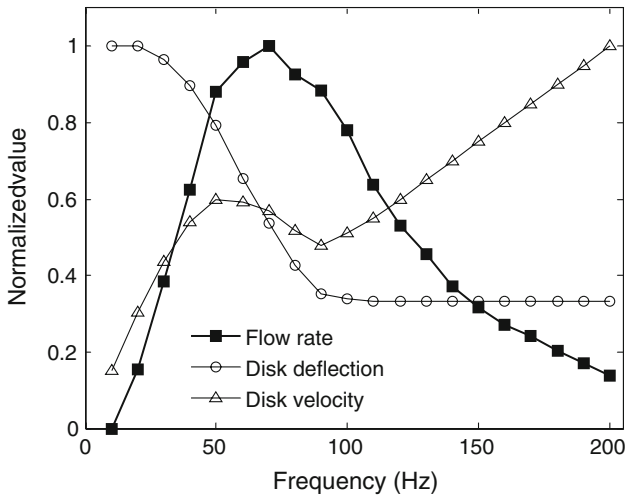

Fig. 6 Measured flow rate, disk deflection, and disk velocity versus frequency at 150 V actuation voltage

pump without water, the disk had a resonance peak at about 4,100 Hz. When the pump was filled with water, the resonance occurred at about 1,000 and 2,800 Hz, respectively, and the resonances became very weak, due to the fluid loading to the disk and high viscosity of water (compared to air). The measurements were carried out for the pumping frequency responses at various actuation voltages. Typical results are plotted in Fig. 6 for the pump at 150 V actuation. In Fig. 6, the disk deflection and its velocity, together with the pumping flowrate are normalized by their maximum values, respectively. It is seen that, at the peak flowrate around 70 Hz, both disk deflections and velocities are actually not at their maxima, indicating that the maximum pumping effects are not produced by large amplitudes of the disk deflection or velocity at this frequency. In other words, the maximum pumping flowrate or backpressure is not controlled by the actuation strength but probably by the flow rectification mechanism associated with the frequencies. We believe that the acoustically featured pump configuration probably attributes to these pump operation frequencies. This is examined in the numerical simulations.

4.2 Numerical simulations and comparisons with experimental results

The experimentally measured disk deflections are input into the numerical model for the actuation amplitude A_0 expressed by Eq. 3, and the numerical simulations were conducted by using FLUENT. Figure 7 shows a comparison of the simulated flowrates with the measured values for the pump actuated at 60 V. General agreements between the simulated flowrates and experimental values are observed. Specifically, both the numerical simulation and

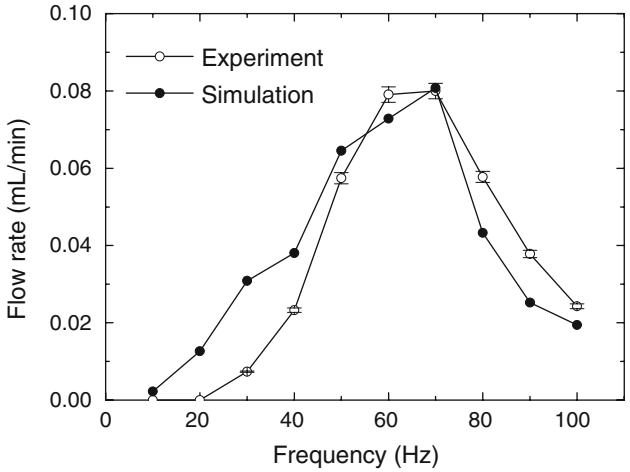

Fig. 7 Comparison of the measured and simulated flow rates versus frequency at 60 V actuation voltage

the experiment show that the maximum flowrates occur at the peak pumping frequency of about 70 Hz. The numerical simulations can also provide the detailed information for the flow fields inside the pumps. Figure 8 shows the transient flow streamlines inside the pump chamber at different four moments in one period T, corresponding to four different disk diaphragm positions. At $t = 1/2T$, the disk diaphragm is at the mid-positions moving downwards to push the fluid out from the pump chambers, while at $t = T$, the disk diaphragm is at the mid-positions moving upwards to suck the fluid into the pump chambers. At these two moments, the flow streamlines inside the buffered pump are similar and symmetric though the fluid is flowing out at $t = 1/2T$ and flowing in at $t = T$. Furthermore, since the diaphragm displacement at these two moments reaches its minimum, the complex interactions among the actuation, fluid dynamics and inertia result in small corresponding fluid velocities, and thus no any vortex is observed. However, it is noted that the flow patterns at $t = 1/4T$ and $t = 3/4T$ are very different. Specifically, vortices are generated near the junctions of the chamber connecting to the straight channel because at these two pumping moments, the diaphragm displacement reaches its maximum, corresponding which the afro-mentioned complex interactions cause fluid velocities to undergo large change around the junctions. A closer examination of those vortices indicated by the magnified dashed rectangles indicates very different flow and vortex patterns at these two moments. The flow patterns in this magnified area show clearly that, at $t = 1/4T$, there are two big vortices accompanied by two small ones, while at $t = 3/4T$, there are only two big vortices. The different flow patterns at these two pumping moments generate the flow rectification and thus the net pumping effect. This is further verified by observing the flow patters at the actuation frequency $f = 500$ Hz and voltage 210 V; under these actuation

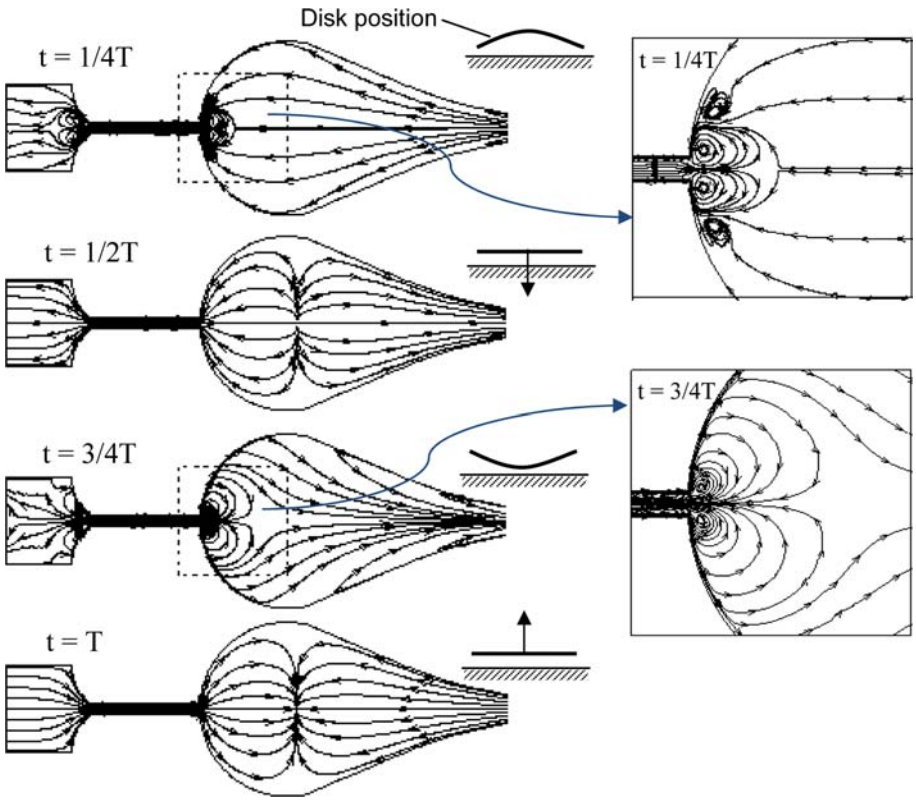

Fig. 8 Flow streamlines inside the pump chamber at four moments in one period T: $t = T/4$ when the disk reaches to the up-most position, $t = T/2$ when the disk moves down in the mid-position, $t = 3/4T$ when the disk reaches to the bottom-most position and $t = T$ when the disk moving up in the mid-position. The pump is driven at frequency 70 Hz and voltage 60 V

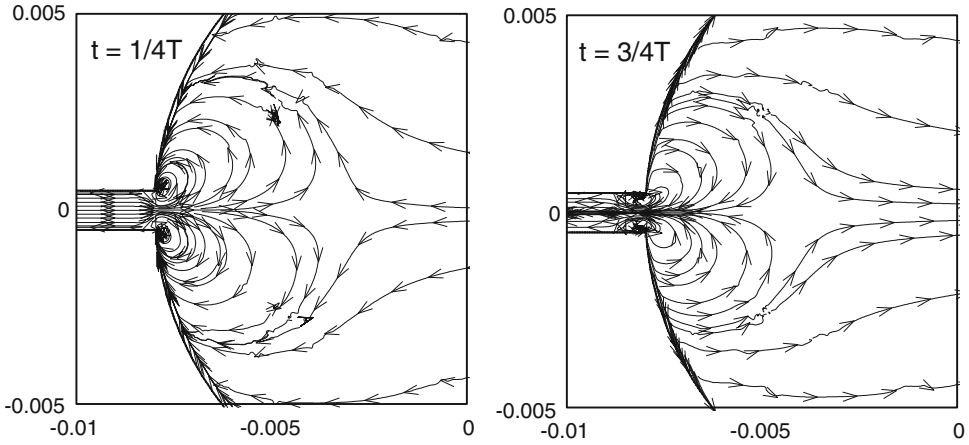

Fig. 9 Detailed flow streamlines inside *dashed rectangular areas* (indicated in Fig. 8) at $t = T/4$ when the disk reaches to the *up-most position*, and $t = 3/4T$ when the disk reaches to the *bottom-most position*. The pump is driven at frequency 500 Hz and voltage 210 V. There is no pumping effect in this case according to the simulation and test

conditions, both the simulation and the experiment confirmed no net pumping effect. The simulated flow streamlines in this case at $t = 1/4T$ and $3/4T$ are depicted in Fig. 9. It is seen that the flow patterns at these two actuation moments are very similar except the flow directions. This explains why there is no flow rectification and thus no pumping effect in this case. In addition, the peak pumping frequency of the pump was further studied by changing the pump dimensions. In the modified pump, shown in Fig. 10a, the 10 mm-straight channel between the end of the nozzle and the buffer area is removed, and the flowrates were computed numerically and measured experimentally. The results presented in Fig. 10b show that the peak pumping frequency occurs at 80 Hz, increased by 14% from the previous peak pumping frequency 70 Hz for the pump shown in Fig. 1b. It is demonstrated that the pumping frequency of the pump developed in this study is indeed dependent on the configuration and dimensions of the pump.

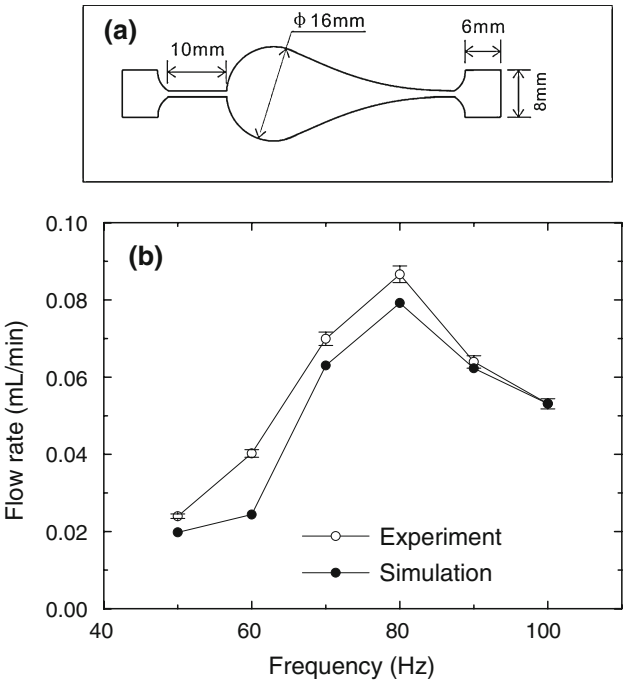

Fig. 10 **a** The modified pump, based on dimensions shown in Fig. 1b, by removing the 10 mm-straight channel at the right from the nozzle end to buffer area. **b** The pumping flowrates by experiment and simulation, showing the peak pumping frequency is at 80 Hz

5 Conclusions

A new design of a valveless micropump has been demonstrated. The pump has an acoustically featured pumping chamber which functions for both flow pumping and rectification. The pump has been studied using both experimental characterizations and numerical simulations. The results have shown that the micropump can produce relatively high flowrates and backpressures, depending on the actuation frequencies and voltages. The maximum pumping effects occur around 70 and 80 Hz for the two pumps with a slight difference in pump configurations and dimensions. It should be pointed out that these effective pumping frequencies are much lower than kilo Hertz reported for other micropumps driven by piezoelectric actuators. The low pumping frequency is caused by the acoustic resonance feature of the pumping system, but not due to the large disk actuations at the peak frequency. The numerical simulations agree qualitatively with the experimental results and can also provide the detailed flow patterns to show the pumping mechanisms. The simple design and low operation frequency make the present pump suitable for microfluidic integrations.

Acknowledgment Wang SS would like to thank the scholarship provided by Nanyang Technological University, Singapore.

References

Gray BL, Jaeggi D, Mourlas NJ et al (1999) Novel interconnection technologies for integrated microfluidic systems. Sens Actuators A 77:57–65

Heschel M, Mullenborn M, Bouwstra S (1997) Fabrication and characterization of truly 3D diffuser/nozzle microstructures in silicon. J Microelectromech Syst 6:41–47

Huang XY, Wen CY and Jiao ZJ (2009) A standing wave model for acoustic pumping effect in microchannels. Appl Acoust. doi: 10.1016/j.apacoust.2009.08.002

Jiang XN, Zhou Z, Huang XY, Li Y, Liu CY (1998) Micro-nozzle/diffuser flow and its application in micro valveless pumps. Sens Actuators A 70:81–87

Laser DJ, Santiago JG (2004) A review of micropumps. J Micromech Microeng 14:R35–R64

Lee CY, Chang HT and Wen CY (2008) A MEMS-based valveless impedance pump utilizing electromagnetic actuation. J Micromech Microeng 18:035044 (9 pp)

Luo C, Huang XY, Nguyen NT (2007) Generation of shock free pressure waves in shaped resonators by boundary driving. J Acoust Soc Am 121:2515–2525

Nguyen NT, Huang XY, Chuan TK (2002) MEMS-micropumps. J Fluids Eng Trans ASME 124:384–392

Olsson A, Stemme G, Stemme E (2000) Numerical and experimental studies of flat-walled diffuser elements for valve-less micropumps. Sens Actuators A 84:165–175

Pan LS, Ng TY, Liu GR, Lam KY, Jiang TY (2001) Analytical solutions for the dynamic analysis of a valveless micropump: a fluid-membrane coupling study. Sens Actuators A 93:173–181

Schwesinger N, Frank T, Wurmus H (1996) A modular microfluidic system with an integrated micromixer. J Micromech Microeng 6:99–102

Smits JG (1990) Piezoelectric micropump with three valves working peristatically. Sens Actuators A 21–23:203–206

Stemme E, Stemme G (1993) A valveless diffuser/nozzle-based fluid pump. Sens Actuators A 39:159–167

Timoshenko S, Woinosky-Krieger S (1959) Theory of plates and shells. McGraw-Hill, NewYork

Van Lintel HTG, Van den Pol FC, Bouwstra MS (1988) A piezoelectric micropum based micromachining of silicon. Sens Actuators 15: 153–167

Wang SS, Jiao ZJ, Huang XY, Yang C and Nguyen NT (2009) Acoustically induced bubbles in a microfluidic channel for mixing enhancement. Microfluid Nanofluid. doi:10.1007/s10404-008-0357-6

Wu JK, Lu LJ (2006) Liquid-solid coupled system of micropumps. Acta Mech Solida 18(4):308–310